International Journal of Engineering, Mathematical and Physical Sciences
ISSN: 2517-9934
Vol:7, No:2, 2013

Bifurcations and Chaotic Solutions of Two-dimensional Zonal Jet Flow on a Rotating Sphere

Eiichi Sasaki, Shin-ichi Takehiro and Michio Yamada

Abstract—We study bifurcation structure of the zonal jet flow the streamfunction of which is expressed by a single spherical harmonics on a rotating sphere. In the non-rotating case, we find that a steady traveling wave solution arises from the zonal jet flow through Hopf bifurcation. As the Reynolds number increases, several traveling solutions arise only through the pitchfork bifurcations and at high Reynolds number the bifurcating solutions become Hopf unstable. In the rotating case, on the other hand, under the stabilizing effect of rotation, as the absolute value of rotation rate increases, the number of the bifurcating solutions arising from the zonal jet flow decreases monotonically. We also carry out time integration to study unsteady solutions at high Reynolds number and find that in the non-rotating case the unsteady solutions are chaotic, while not in the rotating cases calculated. This result reflects the general tendency that the rotation stabilizes nonlinear solutions of Navier-Stokes equations.

Keywords—rotating sphere, two-dimensional flow, bifurcation structure

I. Introduction

IN planetary atmospheres in Jupiter or Saturn, for example, strong zonal jets have been observed. The two-dimensional incompressible Navier-Stokes flow on a rotating sphere has been considered to be one of the simplest and most fundamental models of the atmospheric motions, and attracts many researchers' interests. In this model, non-dimensional parameters determining the dynamics are the Reynolds number and the Rossby number (inverse of the non-dimensional rotating rate of the sphere). In general, as the Reynolds number increases, a fluid motion becomes turbulent and the Reynolds number of the planetary atmospheres is quite huge, the two-dimensional Navier-Stokes turbulence on a rotating sphere has been studied.

Numerical time integrations of the two-dimensional Navier-Stokes turbulence on a rotating sphere was first performed by Williams [1], who investigated the forced two-dimensional turbulence on a rotating sphere under a symmetry assumption of the flow field, and found that zonal jet flows, similar to those of Jovian atmospheres, emerges in a turbulent flow field. His results raised an expectation that the forced two-dimensional flow on a rotating sphere can be a fundamental model to the planetary atmospheres. However, his computational domain was restricted to $1/16$ of the entire sphere under the assumptions of a longitudinal periodicity and the equatorial symmetry.

E. Sasaki is PhD student at Research Institute for Mathematical Sciences, Kyoto University, Kyoto, 606-8502, Japan. (e-mail: esasaki@kurims.kyoto-u.ac.jp).
S. Takehiro and M. Yamada are with Research Institute for Mathematical Sciences, Kyoto University.

Later Yoden and Yamada [2] first studied the asymptotic states of freely decaying two-dimensional turbulence on a rotating sphere with no assumption on the flow field, and showed that circumpolar west-ward strong jets emerge along with multiple weak jets at the low and middle latitudes. Further Takehiro *et al.* [3] showed that as the rotation rate Ω increases, the width of the circumpolar west-ward jets decreases as $\Omega^{-1/4}$ and the velocity of the jets increases as $\Omega^{1/4}$.

As for the forced turbulence, Nozawa and Yoden [4] performed the numerical time integration with Markovian random forcing, and found that at the final stage of their computation, the flow field consists of multiple zonal jet flow and/or west-ward circumpolar jets, depending on the rotation rate and the forcing wavenumber. However, recently, Obuse *et al.* [5] re-calculated the same problem as Nozawa and Yoden with the numerical integration time being more than 100 times of that of Nozawa and Yoden, and found that at an early stage of the time integration, the multiple zonal jet flows and the circumpolar jets are observed, but as time goes on, the zonal jets merge with each other, and at the final stage of the time integration, only two or three broad zonal jets are left in the flow field. The surviving broad jets are found to be quite *stable* to disturbance even in the ambient turbulent flows.

On the stability of the zonal jet flows, Baines [6] studied the inviscid linear stability of the typical zonal jet flows, the streamfunction of which is expressed by a single spherical harmonics Y_l^0, as well as the inviscid Rossby wave solutions. He solved the eigenvalue problem numerically using the spectral method by the spherical harmonics with the truncation wavenumber up to 20. The inflection-point theorem says that the zonal jet is stabilized when the rotation rate is large enough. Therefore the zonal flow has the critical rotation rate at which the zonal jets obtain the stability. He obtained numerically the critical rotation rate of the zonal flows, and found that the critical rotation rates are only slightly different from the estimates obtained from the inflection-point theorem. The numerical calculation of the stability eigenvalues by Baines [6] was significantly challenging at the time prior to the major advance of computational environment, and the obtained values have been frequently employed by many researchers. Recently Sasaki *et al.* [7] however restudied the stability problem as Baines [6], and found that the numerical calculation of the linear stability studied by Baines is difficult even at present because of an emergence of singularities, so-called critical layers. They re-examined the linear stability of the zonal jet flows with a special attention to the numerical methods

for some eigenvalues and corrected the critical rotation rates obtained by Baines [6] up to $\sim 20\%$.

In the viscous flow cases, Sasaki *et al.* [8] studied the linear stability of the *viscous* zonal jet flows. They found that, at the the critical Reynolds number where the zonal jet flow loses the stability, the zonal jet flow becomes Hopf unstable and the critical longitudinal wavenumber is 2 in the non-rotating case. They found that, when the rotation rate increases, the critical Reynolds number of the zonal jet flows increases rapidly, and at high Reynolds number the unstable region of the rotation rate is larger than that for the inviscid zonal flow, and the former does *not* converge to the latter even in the inviscid limit. This seeming contradiction between the inviscid limit and the inviscid cases is resolved by an observation that the growth rates of the unstable modes converge to zero in the regions of the rotation rate where the viscous zonal flow is unstable but the inviscid zonal flow is stable as the Reynolds number increases. They also discussed the stability of the resultant turbulent zonal flow observed by Obuse *et al.* [5] in the linear framework of the laminar flow.

In this paper we study the bifurcation structure arising from the viscous zonal jet flow as the further problem of the linear stability studied by Sasaki, Takehiro and Yamada [8] on the point of the research on nonlinear solutions arising from the viscous zonal flow after the zonal flow becomes linearly unstable.

The stability and bifurcation problem of the viscous zonal flow is formulated by introducing a forcing term, which consists of a single spherical harmonics, to balance with the viscous dissipation term to keep the zonal flow steady (see also [8]). This problem setting is similar to the Kolmogorov problem which has been considered as a typical and fundamental example to get insight into the solution properties of the Navier-Stokes equations. On the Kolmogorov problem the flow field is governed by the two-dimensional incompressible Navier-Stokes equations with a sine type external forcing on a double-periodic domain, flat torus. In our case, on the other hand, the problem is formulated on a two-dimensional sphere, and with the forcing term consisting of a single spherical harmonics function which is an eigenfunction of the Laplacian similar to that of the Kolmogorov problem. Both the problems are formulated on a two-dimensional boundary-less compact manifold with the forcing of the single eigenfunction of Laplacian on each manifold, and are quite similar to each other with a difference in the topology of the flow domain (genus 0 for the sphere, and genus 1 for the torus).

For the Kolmogorov problem, Iudovichi [9] proved that the two-jet parallel flow on a vertically long flat torus is globally asymptotic stable at an arbitrary Reynolds number, and Meshalkin and Sinai [10] proved that the critical modes of the parallel flows are steady (not Hopf), while Iudovich [9] proved the existence of the bifurcation solution arising at the critical stability of the parallel flow. The bifurcation diagram of steady solutions arising from the 2-jet parallel flow was studied by Okamoto and Shōji [11] for several aspect ratios of the flat torus. They found a pitchfork bifurcation arising from the 2-jet parallel flow and also found that as the aspect ratio changes, there appear several types of bifurcations including the saddle-node bifurcation, Hopf bifurcation and the secondary bifurcation. Kim and Okamoto[12] studied the inviscid limit of the steady solutions arising from the 4- and 6-jet parallel flows. In each case the first and the second branches arise through the pitchfork bifurcations, and they found that the flow field of the bifurcating steady solutions consists of multiple vortices around the bifurcation points. However, as the Reynolds number increases along the branches, smaller vortices merge into larger vortices, and the flow field becomes dominated only by one pair of a negative and a positive vortices at high Reynolds number. They called this solution the *unimodal* solution, and suggested that at high Reynolds number there is at least one steady unimodal solution independently of the value of the number of jets of the original parallel flows. Similar phenomena were found also by Okamoto and Shōji [11]. We add that the simplicity of the Kolmogorov problem drives other researches on dynamical system properties such as routes to turbulence [13] and the orbital instability of chaotic flows [14].

In the following, we discuss the bifurcation structure of the zonal jet flows on a rotating sphere and unsteady solutions at high Reynolds number. This paper is constructed as below. In section II, the governing equation is presented. The bifurcation structure of zonal jet flows is discussed in section III. In section IV we discuss unsteady solutions at high Reynolds number. Discussion and conclusion follow in section V.

II. Governing equations

We consider the two-dimensional incompressible Navier-Stokes flows on a rotating sphere governed by the vorticity equation

$$\frac{\partial \Delta\psi}{\partial t} + J(\psi, \Delta\psi) + 2\Omega\frac{\partial \psi}{\partial \lambda} = \frac{1}{R}\left\{(\Delta + 2)\,\Delta\psi + (l(l+1) - 2)\,Y_l^0(\mu)\right\}, \quad (1)$$

where quantities are made non-dimensional and the radius of the sphere is unity. Here t is the time, λ and μ the longitude and the sine latitude $\mu = \sin\phi$ where ϕ is the latitude, ψ the streamfunction and $\Delta\psi = \zeta$ the vorticity, where Δ is the horizontal Laplacian on the unit sphere. The longitudinal and latitudinal components of velocity (u_λ, u_μ) are given by $u_\lambda = -\sqrt{1-\mu^2}(\partial\psi/\partial\mu)$ and $u_\mu = 1/\sqrt{1-\mu^2}(\partial\psi/\partial\lambda)$, respectively. R and Ω are the Reynolds number and a non-dimensional rotation rate of the sphere, respectively, $J(A, B) := (\partial A/\partial\lambda)(\partial B/\partial\mu) - (\partial A/\partial\mu)(\partial B/\partial\lambda)$ the Jacobian and $(l(l+1)-2)Y_l^0(\mu)/R$ the vorticity forcing where $Y_l^m(\lambda, \mu)$ is a 4π-normalized spherical harmonics with the total wavenumber l and the longitudinal wavenumber m. The term of $2\Delta\psi/R$ in the viscosity term is necessary for the conservation of the total angular momentum of the system [15].

The vorticity equation (1) has a steady l-jet zonal flow solution for any Reynolds number and any rotation rate, expressed by

$$\psi_0(\mu) = -\frac{1}{l(l+1)}Y_l^0(\mu), \qquad \zeta_0(\mu) = Y_l^0(\mu), \quad (2)$$

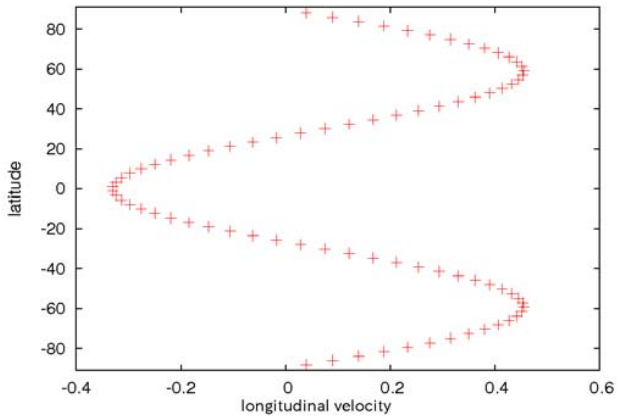

Fig. 1. The longitudinal velocity of the trivial solution. The horizontal and vertical axes indicate the longitudinal velocity and the latitude, respectively.

Here, the number of jets is defined as the number of extreme points of the longitudinal velocity, which is equivalent to the number of nodes of the latitudinal distribution of the streamfunction. We note that on the Kolmogorov problem the two-dimensional Navier-Stokes flow on a flat torus is driven by the vorticity forcing $n^2 \cos ny/R$ and has a $2n$-jet parallel flow solution the streamfunction of which is expressed by $-\cos(ny)/n^2$. The trigonometric function $\cos ny$ is the eigenfunction of Laplacian on the flat torus while the spherical harmonics $Y_l^0(\mu)$ is the eigenfunction of Laplacian on the sphere. Thus this problem setting is similar to the Kolmogorov problem.

III. Bifurcation structure of the zonal jet flow

The 1-jet zonal flow ($l = 1$) corresponds to the conservation of the total angular velocity and the 2-jet zonal flow ($l = 2$) is globally asymptotic stable at arbitrary Reynolds number and rotation rate proved by Sasaki, Takehiro and Yamada [16]. The linear stability of the 3-jet zonal flow ($l = 3$) is studied by Sasaki, Takehiro and Yamada [8], and they found that at high Reynolds number the 3-jet zonal flow is Hopf unstable in the interval $-5.727 < \Omega < 2.171$. In this section, we show the bifurcation structure arising from the the 3-jet zonal flow in the interval of $1 \leq R \leq 10^3$ and in the case of $\Omega = 0.0, \pm 0.5$. As below we call the 3-jet zonal flow the trivial solution. Fig. 1 shows the longitudinal velocity of the trivial solution.

In order to solve the problem numerically, we use the spectral method by the spherical harmonics and assume that the streamfunction ψ is expressed by

$$\psi(\lambda, \mu) = \sum_{n=1}^{N} \sum_{m=-n}^{n} \psi_n^m Y_n^m(\lambda, \mu),$$

where ψ_n^m is the expansion coefficient and N is the truncation wavenumber. We adopt the transform method to evaluate the nonlinear term of the equation (1), with, in the physical space, the number of the longitudinal and latitudinal grid points I and J satisfying $I \geq 3N + 1$ and $J > 3N/2$ eliminating aliasing errors. We seek to nonlinear steady solutions using the Newton method. The stopping condition of the Newton method is that the maximum absolute value of correction of the real/imaginary part of the spectral components is less than 10^{-8} with checking the accuracy by changing the truncation wavenumber up to $N = 106$.

A. Bifurcation diagram in the non-rotating case

The nonlinear steady solutions arising from the trivial solution are *Traveling Wave* solutions thought the Hopf bifurcation at the critical Reynolds number of the trivial solution where the trivial solution becomes Hopf unstable. Furthermore, we find that all bifurcating steady solutions are traveling wave solutions. Therefore we call these solutions as TW with serial characters.

We find that TW1 ($m = 2$) bifurcates from the trivial solution at $R = 26.123$ through the super-critical Hopf bifurcation. Fig. 2 shows the bifurcation diagram. Tracing TW1 branch, we find two secondary pitchfork bifurcation points at $R = 70.66$ and 203.8. At $R = 70.66$, where TW1 losses the linearly stability, TW2-N and TW2-S bifurcate though the pitchfork bifurcation. We find that TW2-N has two negative vortices at the mid-latitudes in the *northern* hemisphere while TW2-S has two positive vortices at the mid latitudes in the *southern* hemisphere. The flow field of TW2-N and TW2-S is antisymmetric with respect to the equator. Notice that -N and -S indicate the hemisphere where the solution has large vortices. As the Reynolds number increases, TW2-N and TW2-S become Hopf unstable at $R = 103.2$. On TW1 branch we find that, as the Reynolds number increases, TW1 recovers linearly stable again at $R = 203.8$ where TW3-N and TW3-S bifurcate through the pitchfork bifurcation. We confirm that TW3-N and TW3-S are Hopf unstable for the interval of $203.8 \leq R \leq 10^3$. As the Reynolds number further increases, TW1 becomes Hopf unstable again at $R = 249.4$. On the trivial solution we find that TW4 ($m = 1$) bifurcates at $R = 62.51$ through Hopf bifurcation, and confirm that TW4 is Hopf unstable for the interval of $62.5 \leq R \leq 10^3$. On TW4 branch, we find that TW5-N and TW5-S bifurcate at $R = 136.2$ through the pitchfork bifurcation, and TW5-N and -S are Hopf unstable except for the interval of $143.5 \leq R \leq 161.9$, both ends of which are considered to be associated with bifurcations of time-periodic solutions.

All secondary bifurcation points in our computation are pitchfork and all the steady/steady traveling solutions (where the steady solution means the trivial solution) become Hopf unstable until at $R = 249.4$. Finally we note that, as the Reynolds number increases, the absolute value of phase velocity of the steady traveling solutions decreases monotonically.

B. Bifurcation diagram in the rotating case

Fig. 3 shows the bifurcation diagram in the case of $\Omega = -0.5$. We find that as the Reynolds number increases the trivial solution becomes Hopf unstable at $R = 26.58$ where TW1 ($m = 2$) bifurcates through the super-critical Hopf bifurcation. As the Reynolds number further increases TW1 becomes Hopf unstable at $R = 81.08$. On the trivial solution we find another Hopf bifurcation point at $R = 48.15$ where TW4 ($m = 1$)

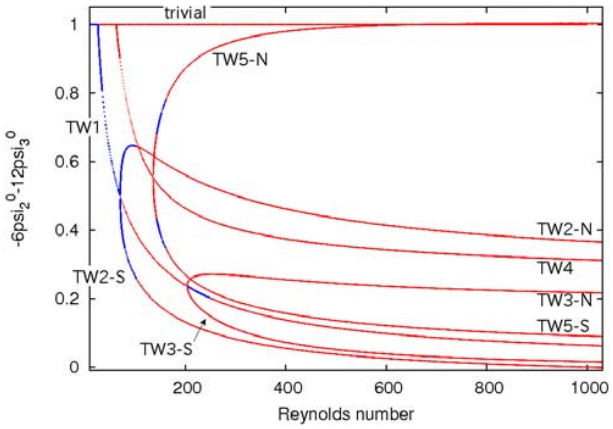

Fig. 2. Bifurcation diagram of the steady/steady traveling solutions in the non-rotating case, $\Omega = 0$. The blue asterisks and red crosses denote that the solutions are linearly stable and linearly unstable, respectively. The horizontal and vertical axes indicate the Reynolds number and $-6\psi_2^0 - 12\psi_3^0$, respectively.

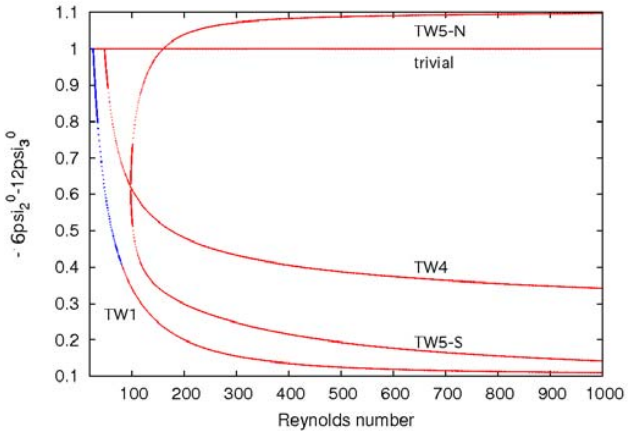

Fig. 3. Same as Fig. 2 but in the case of $\Omega = -0.5$. The horizontal and vertical axes indicate the Reynolds number and $-6\psi_2^0 - 12\psi_3^0$, respectively.

bifurcates. We confirm that TW4 is Hopf unstable for the interval of $48.15 \leq R \leq 10^3$. On TW4 branch we find that TW5-N and TW5-S bifurcate at $R = 98.57$ though the pitchfork bifurcation and confirm that TW5-N and TW5-S are Hopf unstable for the interval of $98.57 \leq R \leq 10^3$.

Fig. 4 shows the bifurcation diagram in the case of $\Omega = 0.5$. We find that as the Reynolds number increases the trivial solution becomes Hopf unstable at $R = 27.35$ where TW1 bifurcates through the super-critical Hopf bifurcation. Tracing TW1 branch, we find that TW1 becomes Hopf unstable at $R = 60.16$, and a pitchfork bifurcation point at $R = 63.46$ where TW2-N and TW2-S bifurcate. We confirm that TW2-N and TW2-S are Hopf unstable except for the interval of $64.918 \leq R \leq 85.036$. On the trivial solution we find another Hopf bifurcation point at $R = 113.7$ where TW4 bifurcates and confirm that TW4 is also Hopf unstable for the interval of $113.7 \leq R \leq 10^3$. As the Reynolds number further increases we find that TW5-N and TW5-S bifurcate from TW4 at $R =$

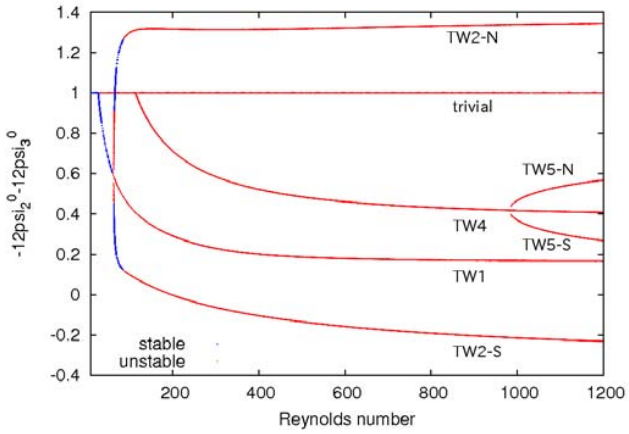

Fig. 4. Same as Fig. 2 , but in the case of $\Omega = 0.5$. The horizontal and vertical axes indicate the Reynolds number and $-12\psi_2^0 - 12\psi_3^0$, respectively.

983.6 through the pitchfork bifurcation and TW5-N and TW5-S are also Hopf unstable for the interval of $983.6 \leq R \leq 10^3$.

Under the stabilizing effect of rotation, as the absolute value of the rotation rate increases, the number of bifurcating solutions at high Reynolds number decreases monotonically. These results suggests that the bifurcation structure changes drastically, as the absolute value of the rotation rate increases.

IV. Numerical simulations at high Reynolds number under 3-jet zonal forcing

We carry out the numerical time integration at $\Omega = 0.0, \pm 0.5$ and $R = 10^3$. We employ the spectral method as same as the before section but the truncation wavenumber is fixed on $N = 53$ (for the grid points $I = 160$ and $J = 80$). The time integration is performed with the forth order Runge-Kutta method with a time step interval $\delta t = 0.05$ from several initial conditions which are obtained by each steady/steady traveling solution added with three different small disturbances expressed by

$$\delta\psi_i(\lambda, \mu) = \sum_{n=2}^{10} \sum_{m=-n}^{n} \delta\psi_{in}^m Y_n^m(\lambda, \mu)$$

where $\delta\psi_{in}^m$ is the expansion coefficient in which the uniform random number are substituted with the energy density of $\delta\psi_i$ equal to 10^{-4} times of that of the original steady/steady traveling solution. Here the energy density of ψ is defined by

$$E = -\frac{1}{8\pi} \int \psi \Delta\psi \, dS.$$

We carry out the time integration until $t = 5 \times 10^5$ and calculate several statistical quantity in the time interval of $5 \times 10^4 \leq t \leq 5 \times 10^5$.

Fig. 5 shows the time series of the energy density of the unsteady solution and Fig. 6 shows the power spectrum of the energy density of the unsteady solution. The energy density undergo intermittent bursts and its power spectrum is broad. Thus the unsteady solution is chaotic. We find that there are many times when the streamfunction of the chaotic solution

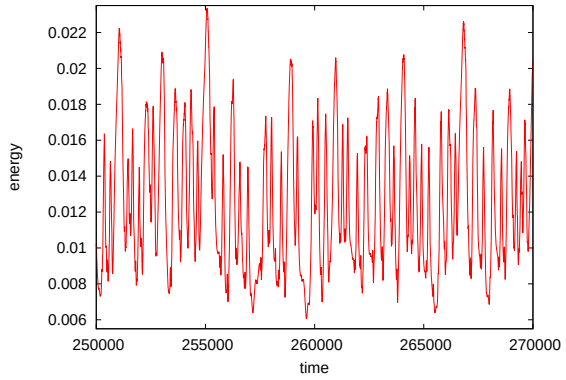

Fig. 5. The time series of the energy density of the chaotic solution at $\Omega = 0.0, R = 10^3$ The horizontal and vertical axes indicate the time and the energy density, respectively.

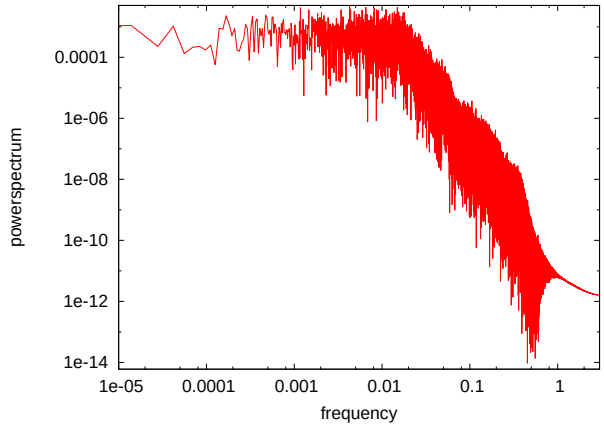

Fig. 6. The power spectrum of the energy density of the chaotic solution in the case of $\Omega = 0.0$ and $R = 10^3$. The horizontal and vertical axes indicate the frequency and the power spectrum, respectively.

is similar to each unstable steady traveling solution and the chaotic solution seems to wander around the unstable steady traveling solutions.

Fig. 7 shows the time-averaged zonal-mean zonal velocity of the chaotic solution with the snapshots of the zonal-mean zonal velocity, where the zonal-mean zonal velocity is defined by

$$U(\mu) = \frac{1}{2\pi} \int_0^{2\pi} u_\lambda(\lambda, \mu)\, d\lambda.$$

The zonal-mean zonal velocity of the chaotic solution is equatorial asymmetry but the time-averaged zonal-mean zonal velocity has equatorial symmetry. This means that the chaotic solution goes through the equatorial asymmetric states where the northern (southern) jet of the zonal-mean zonal velocity is stronger than the southern (northern) jet by the approximately same frequencies. The number of jets of the time-averaged zonal-mean zonal velocity is 3 which is equal to that of the trivial solution but the magnitude of the time-averaged zonal-mean zonal velocity is $\sim 1/5$ of that of the trivial solution.

In the rotating case, on the other hand, Fig. 8 shows the power spectrum of the unsteady solutions at $\Omega = \pm 0.5$ and

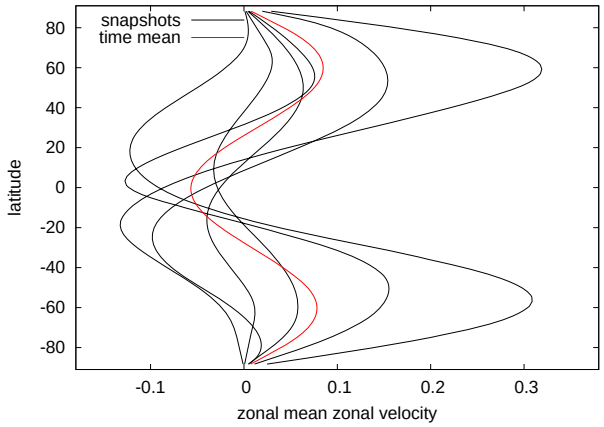

Fig. 7. The zonal-mean zonal velocity in the case of $\Omega = 0.0$ and $R = 10^3$. The red line denotes the time-averaged zonal-mean zonal velocity of the chaotic solution, while the black lines denote the snapshots of the zonal-mean zonal velocity of the chaotic solution, respectively. The horizontal and vertical axes indicate the zonal-mean zonal velocity and the latitude, respectively.

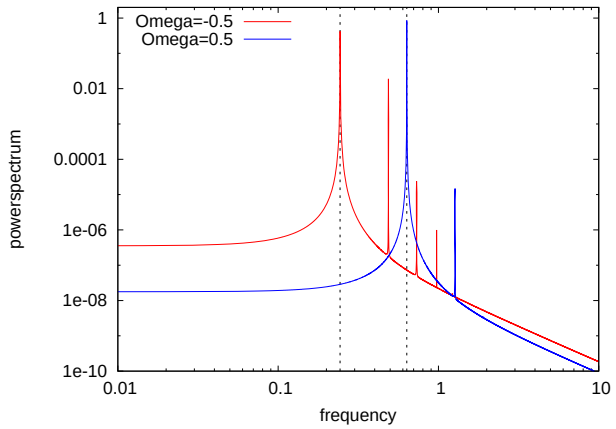

Fig. 8. Same as Fig. 6 but in the cases of $\Omega = \pm 0.5$ and $R = 10^3$. The red and blue lines denote the case of $\Omega = -0.5$ and $\Omega = 0.5$, respectively. The vertical dashed lines indicate $\omega_{-0.5} = 0.243$ and $\omega_{0.5} = 0.635$, respectively.

$R = 10^3$. In the case of $\Omega = -0.5$ the picks of the power spectrum are at the integer multiple of $\omega_{-0.5} = 0.243$ while in the case of $\Omega = 0.5$ the picks are at the integer multiple of $\omega_{0.5} = 0.635$. Thus the unsteady solutions are time-periodic in the each case.

Fig. 9 shows the zonal-mean zonal velocity of the time-periodic solution in the case of $\Omega = -0.5$. The magnitude of the time-averaged zonal-mean zonal velocity of the time-periodic solution is larger than that of the chaotic solutions in the non-rotating case. The northern jet of the time-averaged zonal-mean zonal velocity of the time-periodic solution is slightly larger than the southern jet. Thus the time-averaged zonal-mean zonal velocity of the time-periodic solution is equatorial asymmetric. We also find the time-periodic solutions the southern jet of which is slightly larger than the northern jet and these time-periodic solutions are antisymmetric with respect to the equator.

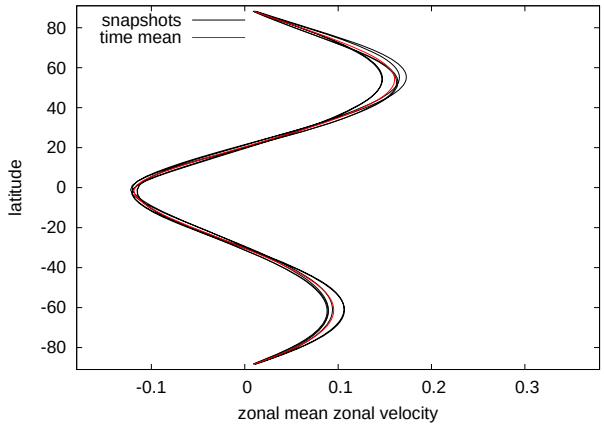

Fig. 9. Same as Fig. 7 but in the case of $\Omega = -0.5$ and $R = 10^3$.

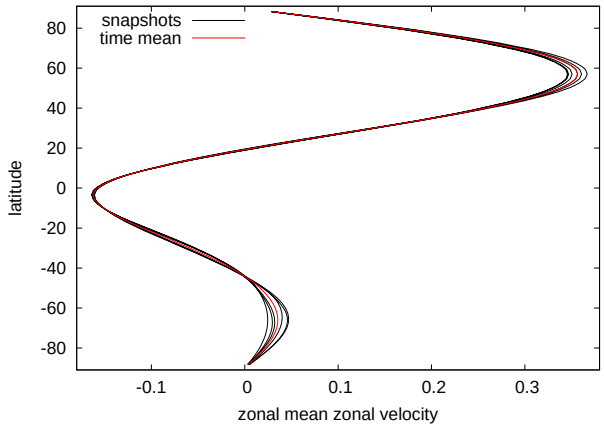

Fig. 10. Same as Fig. 7 but in the case of $\Omega = 0.5$ and $R = 10^3$.

Fig. 10 shows the zonal-mean zonal velocity of the time-periodic solution in the case of $\Omega = 0.5$. The northern jet of this periodic solution is clearly larger than the southern jet. The time averaged zonal-mean zonal velocity of the time-periodic solution in the case of $\Omega = 0.5$ is also equatorial asymmetric. We also find the periodic solutions the northern jet of which is clearly larger than the northern jet and these time-periodic solutions are antisymmetric with respect to the equator.

In the rotating case calculated, the unsteady solutions are the time-periodic even at high Reynolds number where the unsteady solutions are chaotic in the non-rotating case, and the time-averaged zonal-mean zonal velocity of the time-periodic solutions is equatorial asymmetric.

V. Conclusion

In this paper we study the bifurcation structure arising from the zonal flow and the properties of the unsteady solutions at high Reynolds number. On the bifurcation analysis, in the non-rotating case, as Reynolds number increases, the steady traveling solutions arise from the zonal flow through Hopf bifurcation. As the Reynolds number further increases, several traveling solutions arise through the pitchfork bifurcation from the steady traveling solutions and at high Reynolds number the steady/steady traveling solutions become Hopf unstable. In the rotating cases calculated, at high Reynolds number the number of the steady traveling solutions bifurcating from the zonal flow decreases monotonically for the stabilizing effect of rotation.

We also carry out the time integration at $R = 10^3$. In the non-rotating case we find that the unsteady solution is chaotic, and the time-averaged zonal-mean zonal velocity is equatorial symmetric but the time series of the zonal-mean zonal velocity of the chaotic solution is equatorial asymmetric. This result suggests that the chaotic solution has the equatorial asymmetric states by the approximately same frequencies. In the rotating case, on the other hand, the unsteady solutions are time-periodic. The time-averaged zonal-mean zonal velocity of the time-periodic solutions is equatorial asymmetric. These results suggests that the rotation effect stabilizes the nonlinear solutions and the properties of the nonlinear solutions arising from the zonal jet flow change significantly depending on the rotation rate.

It should be noted that in the non-rotating case we find the many times when the streamfunction of the chaotic solution is similar to that of unstable steady/steady traveling solutions obtained by bifurcation analysis. The chaotic solution seems to wander around the unstable steady traveling solutions. Observing the streamfunctions, we expect that properties of the chaotic solutions can be obtained by using unstable steady/steady traveling solutions. As an example, we reproduce the zonal-mean zonal velocity of the chaotic solution using those of the steady/steady traveling solutions by the linear mapping from the solution space to the zonal-mean zonal profiles. The detailed discussion on the reproduction of the zonal-mean zonal velocity of the chaotic solution will be given in Sasaki, Takehiro and Yamada [16].

Acknowledgment

In the numerical calculation of spectral method we use a spectral transformation library “ISPACK” [17] and a FORTRAN90 wrapper library “SPMODEL” [18].

References

[1] P. G. Williams, Planetary circulations: 1. Barotropic representation of Jovian and Terrestrial turbulence *J. Atmos. Sci.*, **35**, 1399–1426, 1978.
[2] S. Yoden, S. and M. Yamada, A numerical experiment on two-dimensional Decaying turbulence on a rotating sphere. *J. Atmos. Sci.*, **50**, 631–643, 1993.
[3] S. Takehiro, S., M. Yamada and Y-Y. Hayashi, Circumpolar jets emerging in two-dimensional non-divergent decaying turbulence on a rapidly rotating sphere. *Fluid Dyn. Res.*, **39**, 209–220, 2007.
[4] T. Nozawa and S. Yoden, Formation of zonal band structure in forced two-dimensional turbulence on a rotating sphere, *Phys. Fluid* , **9**, 2081–2093, 1997.
[5] K. Obuse, S. Takehiro and M. Yamada, Long-time asymptotic states of forced two-dimensional barotropic incompressible flows on a rotating sphere. *Phys. Fluid*, **22**, 056601, 2010.
[6] Baines, P. G., 1976 The stability of planetary waves on a sphere. *J. Fluid Mech.* **73-2**, 193–213.
[7] E. Sasaki, S. Takehiro, and M, Yamada, A note on the stability of inviscid zonal jet flows on a rotating sphere, *J. Fluid Mech.*, **710**, 154–165, 2012.
[8] E. Sasaki, S. Takehiro and M. Yamada, Stability of two-dimensional viscous zonal jet flows on a rotating sphere, in preparation.

[9] I. V. Iudovisch, Example of the generation of a secondary stationary or periodic flow when there is loss of stability of the laminar flow of a viscous incompressible fluid. *J. Appl. Math. Mech.*, **29**, 527–544, 1965.
[10] D. L. Meshalkin and Y. G. Sinai, 1962 Investigation of the stability of a stationary solution of a system of equations for the plane movement of an incompressible viscous liquid, *J. Appl. Math. and Mech.*, **25**, 1700–1705, 1962
[11] H. Okamoto and M. Shōji, Bifurcation Diagrams in Kolmogorov's Problem of Viscous Incompressible Fluid on 2-D Flat Tori. *Japan J. Indus Appl. Math.*, **10**, 191–218, 1993.
[12] C. S. Kim, S. C. and H. Okamoto, Stationary vortices of large scale appearing in 2D Navier-Stokes equations at large Reynolds numbers. *Japan J. Indust. Appl. Math.*, **27**, 47–71, 2010.
[13] N. Platt, L. Sirovich and N. Fitzmaurice, An investigation of chaotic Kolmogorov flows. *Phys. Fluid* , **3**, 681–696, 1991.
[14] M. Inubushi, M. U. Kobayashi, S. Takehiro and M. Yamada, Covariant Lyapunov analysis of chaotic Kolmogorov flows. *Phys. Rev. E* **85**, 016331, 2012.
[15] I. Silberman, Planetary waves in the atmosphere, *J. Meteo.*, **11**, 27–34, 1953.
[16] E. Sasaki, S. Takehiro and M. Yamada, Bifurcation structure of two-dimensional viscous zonal jet flows on a rotating sphere, in preparation.
[17] K Ishioka, ispack-0.96, http://www.gfd-dennou.org/arch/ispack/, GFD Dennou Club, 2011.
[18] S. Takehiro, Y. SASAKI, Y. Morikawa, K. Ishioka, M. Odaka, O. Y. Takahashi, S. Nishizawa, K. Nakajima, M. Ishiwatari, and Y.-Y, Hayashi, SPMODEL Development Group, Hierarchical Spectral Models for GFD (SPMODEL), http://www.gfd-dennou.org/library/spmodel/, GFD Dennou Club, 2011.